
Assessing the accuracy and efficiency of different order implicit and explicit integration schemes

Author 1

- Martí Lloret-Cabot, Ph.D
- Durham University, United Kingdom

Author 2

- Daichao Sheng, Prof
- University of Technology Sydney, Australia

Corresponding author
Martí Lloret Cabot
Marti.lloret-cabot@durham.ac.uk
Department of Engineering
University of Durham
Lower Mount Joy
South Road
Durham
DH1 3LE
Tel: +44 (0) 191 334 1700

ABSTRACT

A first order accurate fully implicit integration scheme and four different order explicit substepping integration schemes with automatic error control are used in this paper to integrate the constitutive relations of a critical state model for saturated soils. Their respective computational performance in terms of accuracy and efficiency is assessed in order to provide practical guidance for deciding which of the five is most suitable for solving numerical problems in geotechnical engineering involving critical state models. Even though existing literature of integration schemes applied to geotechnical problems has traditionally been focussed on the first order accurate implicit backward Euler and on the second order accurate explicit modified Euler with substepping almost exclusively, the findings of this paper suggest that the little extra work required in the implementation of an explicit third order Runge-Kutta substepping scheme is worth the effort, especially in terms of computational cost.

1. INTRODUCTION

In numerical analysis of geotechnical problems, the mechanical response of the soil is governed by the stress-strain relations of a constitutive model (Alonso et al., 1990; Lloret-Cabot et al., 2017a, 2018ab; Roscoe & Burland, 1968). The numerical integration of such constitutive relations is a challenging task because of the highly non-linear behaviour often encountered in geotechnical engineering. Many different strategies have been proposed for an efficient numerical integration of the stress-strain relations of a soil model, and these are commonly grouped as implicit (stresses are updated from the stress state at the end of the strain increment by using a sort of iterative procedure) (Belytschko et al., 2000; Borja and Tamagnini, 1998; Coombs et al., 2010, 2011; Jeremic & Sture, 1997; Pérez-Foguet et al., 2001ab; Simo & Taylor, 1986) and explicit (stresses are computed from the stress state at the start of the strain increment) (Farias et al., 2009; Lloret-Cabot et al., 2016; Pérez-Foguet et al., 2001a; Sloan, 1987; Sloan et al., 2001).

Accuracy and efficiency of an integration scheme are both central to the overall precision and cost involved in finite element applications (Potts, 2003; Sloan et al., 2001). Hence, comparisons between implicit and explicit integration schemes have been an interesting topic of discussion (e.g. Pedroso & Farias, 2005; Potts & Ganendra, 1994). In order to provide practical guidance on their suitability for finite element analysis, the work presented here studies the computational performance of five integration schemes, including the fully implicit first order accurate backward Euler and a family of different order accurate explicit substepping schemes with automatic error control.

Since the work of Sloan (1987), substepping integration schemes (sometimes also called embedded or adaptive methods) have been used in geotechnical engineering to integrate constitutive models for soils, involving saturated (e.g. Abbo & Sloan, 1996; Farias et al., 2009; Lloret-Cabot et al., 2016; Pedroso & Farias, 2005; Pérez-Foguet et al., 2001ab; Quevedo et al., 2019; Sheng et al., 2002;Sloan et al., 2001; Zhao et al. 2005; Zhao et al., 2017) as well as unsaturated conditions (e.g. Cattaneo et al., 2014; Lloret-Cabot et al., 2021; Pedroso et al., 2008; Sheng et al., 2003ab; Sołowski & Gallipoli, 2010ab; Sołowski et al., 2012; Zhang & Zhou, 2016). In contrast to the conventional single-step explicit or fully implicit schemes (in which the size of the

integration step is not directly controlled) the advancement of the solution in an explicit substepping scheme is controlled by estimating the local truncation error. This estimation is possible by *embedding* a lower order single-step accurate scheme in a higher order single-step scheme. The difference in the numerical solutions from these two schemes gives the estimate of the local error that is used by the substepping algorithm to adjust the size of the integration substep, making the overall process of integration more efficient than single-step explicit or implicit approaches (Sloan et al., 2001).

Traditionally, the use of implicit and explicit integration schemes in geotechnical engineering has concentrated on the implicit first order backward Euler and on the explicit second order modified Euler with substepping almost exclusively, with little research on the performance of higher order integration substepping schemes (e.g. Sołowski et al., 2012). The goal of this paper is then to answer the following question: are traditional integration schemes as good as they can be for solving geotechnical engineering problems, or is there the possibility for improvement?

To answer this question, a thorough investigation of the numerical performance and computational cost involved in the numerical integration of a critical state model for saturated soils is carried out for five integration schemes, including the first order accurate implicit backward Euler (BE1), the second order Runge-Kutta with substepping (RK12), the third order Runge-Kutta with substepping (RK23), the fourth order Runge-Kutta with substepping (RK34) and the fifth order Runge-Kutta with substepping (RK45). The analysis of the results from these five integration schemes shows that, for a given accuracy, a substantial reduction in computational cost can be achieved at the expense of the extra effort required in implementing a higher order method.

2. FORMULATION OF THE PROBLEM

The numerical integration of a critical state model requires the solution of an ordinary differential system of equations that needs to be solved numerically via an integration scheme (Sloan et al., 2001). Without loss of generality, the next sections investigate the problem for the Modified Cam Clay (MCC) (Roscoe & Burland, 1968) but similar outcomes are expected for more advanced models of the critical state family. According

to Sloan et al. (2001) the system of ordinary differential equations to be solved can be written as:

$$\begin{cases} \mathrm{d}\boldsymbol{\sigma}' = \mathbf{D}\mathrm{d}\boldsymbol{\varepsilon} \\ \mathrm{d}p'_0 = \mathrm{d}\lambda B \\ \mathrm{d}v = -v\mathrm{d}\varepsilon_v \end{cases} \quad (1)$$

where d$\boldsymbol{\sigma}'$ is the effective stress vector (defined as the difference between the total stress and pore water pressure), d$\boldsymbol{\varepsilon}$ is the strain vector, $\mathbf{D}$ is the elastic matrix $\mathbf{D_e}$ (if no plastic yielding occurs) or the elasto-plastic matrix $\mathbf{D_{ep}}$ (when the given strain increment causes plastic yielding, dp_0' is the mechanical hardening parameter, dλ is an unknown positive scalar (referred to as the plastic multiplier), B is a scalar function for the evolution of the yield curve, v is the specific volume and dε_v is the volumetric strain (see Sloan et al. (2001) and Lloret-Cabot et al. (2016) for more details).

Equation 1 defines an initial value problem (IVP) to be solved via an integration scheme when knowing the variation of strain, the initial effective stresses and the initial hardening parameter.

Five different order integration schemes are presented in the next sections to solve Equation 1, including the second order accurate explicit modified Euler with substepping (RK12) together with a third, a fourth and a fifth order accurate explicit Runge-Kutta substepping schemes (RK23, RK34 and RK45, respectively) and the implicit first order backward Euler (BE1).

3. EXPLICIT SUBSTEPPING INTEGRATION SCHEMES

This section summarises the four explicit substepping strategies with automatic error control used to integrate Equation 1. Full details on explicit substepping algorithms, including elastic-plastic transitions, yield curve intersection and correction of stresses back to the yield surface (see Potts & Gens, 1985) is given elsewhere (e.g. Sloan et al., 2001).

To solve Equation 1, it is useful to define a pseudo-time T, with $T = 0$ at the start of the strain increment $\Delta\boldsymbol{\varepsilon}$ and $T = 1$ at the end:

137 $$\begin{cases} \dfrac{\mathrm{d}\boldsymbol{\sigma}'}{\mathrm{d}T} \cong \mathbf{D}_{\mathbf{ep}}\Delta\boldsymbol{\varepsilon} = \mathbf{D}_{\mathbf{e}}\Delta\boldsymbol{\varepsilon} - \Delta\lambda\mathbf{D}_{\mathbf{e}}\mathbf{b} \\ \dfrac{\mathrm{d}p'_0}{\mathrm{d}T} \cong \Delta\lambda B \\ \dfrac{\mathrm{d}v}{\mathrm{d}T} = -v\Delta\varepsilon_{\mathrm{v}} \end{cases} \quad (2)$$

138 where

139 $$\Delta\lambda = \frac{\mathbf{a}^T\mathbf{D}_{\mathbf{e}}\Delta\boldsymbol{\varepsilon}}{A - \mathbf{a}^T\mathbf{D}_{\mathbf{e}}\Delta\mathbf{b}} \quad (3)$$

140 where **a** and **b** are, respectively, the derivative of the yield curve and plastic potential
141 with respect to effective stress and A is a scalar related to the hardening law (Sloan et
142 al., 2001) (note that the subscript ^{T} means transposed).

143 Equation 2 is the IVP to be integrated with the substepping scheme over T, when
144 knowing the initial state of the soil at $T = 0$ and the imposed increment of strain $\Delta\boldsymbol{\varepsilon}$.
145 Given a pseudo-time substep ΔT_n (with $T \in (0, T_{n-1}]$), the updates for $\boldsymbol{\sigma}'$, p'_0 and v can
146 be written as:

147 $$\begin{cases} \boldsymbol{\sigma}'_n = \boldsymbol{\sigma}'_{n-1} + \sum_{i=1}^{s} b_i \Delta\boldsymbol{\sigma}'_i \\ p'_{0n} = p'_{0n-1} + \sum_{i=1}^{s} b_i \Delta p'_{0i} \\ v_n = v_{n-1}\exp\left(-\Delta T_n \Delta\varepsilon_v\right) \end{cases} \quad (4)$$

148 where s is the number of stages of the integration scheme, the coefficients b_i take
149 different values depending on the susbtepping scheme used (see Tables 1, 2, 3 and 4
150 for RK12, RK23, RK34 and RK45 respectively) and

151 $$\left.\begin{array}{l} \Delta\boldsymbol{\sigma}'_i = \mathbf{D}_{\mathbf{ep}}\left(\hat{\boldsymbol{\sigma}}'_i, \hat{p}'_{0i}, \hat{v}_i\right)\Delta\boldsymbol{\varepsilon}_n \\ \Delta p'_{0i} = \Delta\lambda\left(\hat{\boldsymbol{\sigma}}'_i, \hat{p}'_{0i}, \hat{v}_i, \Delta\boldsymbol{\varepsilon}_n\right) B\left(\hat{\boldsymbol{\sigma}}'_i, \hat{p}'_{0i}, \hat{v}_i\right) \\ \Delta\boldsymbol{\varepsilon}_n = \Delta T_n \Delta\boldsymbol{\varepsilon} \end{array}\right\} \quad \text{for } i = 1, \ldots, s \quad (5)$$

152 with

153
$$\left.\begin{aligned} \hat{\boldsymbol{\sigma}}'_i &= \boldsymbol{\sigma}'_{n-1} + \sum_{k=1}^{i-1} a_{ik} \Delta \boldsymbol{\sigma}'_k \\ \hat{p}'_{0i} &= p'_{0n-1} + \sum_{k=1}^{i-1} a_{ik} \Delta p'_{0k} \\ \hat{v}_i &= v_{n-1} \exp\left(-\sum_{k=1}^{i-1} a_{ik} \Delta T_n \Delta \varepsilon_v \right) \end{aligned}\right\} \quad \text{for } i = 1, ..., s \tag{6}$$

154 and the coefficients a_{ik} take different values depending on the susbtepping scheme used
155 (see the corresponding Butcher tableau below).

156 In all substepping schemes considered in this paper, the estimate of the local truncation
157 error *REL* used to adjust the size of the substep $\delta\boldsymbol{\varepsilon}$ is computed as:

158
$$REL = max\left\{ \frac{\left[\left(\hat{\boldsymbol{\sigma}}' - \boldsymbol{\sigma}' \right)^T \left(\hat{\boldsymbol{\sigma}}' - \boldsymbol{\sigma}' \right) \right]^{1/2}}{\left[\left(\hat{\boldsymbol{\sigma}}' \right)^T \left(\hat{\boldsymbol{\sigma}}' \right) \right]^{1/2}}, \frac{\left| \hat{p}_0' - p_0' \right|}{\hat{p}_0'} \right\} \tag{7}$$

159 where the variables with a hat correspond to the higher order accurate approximations
160 of the substepping scheme.

161 If *REL* is larger/smaller than a specified substepping tolerance *STOL*, the current size
162 of the integration step/substep is reduced/increased according to:

163
$$\left(\Delta T \right)_{i+1} = r \left(\Delta T \right)_i \tag{8}$$

164 where *r* is a scalar.

165 The value of *r* is bounded between 0.1 and 1.1 to control the change in size during two
166 consecutive substeps (Sloan et al., 2001) and its expression depends on the accuracy of
167 the substepping scheme. For the RK12, RK23, RK34 and RK45 the expression of *r* is,
168 respectively:

169
$$r \cong 0.9 \left(STOL / REL \right)^{1/2} \tag{9}$$

170
$$r \cong 0.9 \left(STOL / REL \right)^{1/3} \tag{10}$$

$$r \cong 0.9\left(STOL/REL\right)^{1/4} \tag{11}$$

$$r \cong 0.9\left(STOL/REL\right)^{1/5} \tag{12}$$

All the substepping schemes considered in this paper use *local extrapolation*, meaning that if the step/substep is accepted, the values of the effective stresses, and hardening parameter (the end of the step/substep) are updated using the higher order approximation (Shampine, 1973).

Table 1 indicates the values of the coefficients b_i and a_{ik} for Equations 4 and 6, respectively, corresponding to the second order Runge-Kutta scheme with substepping (RK12). The RK12 embeds the first order accurate single-step forward Euler (RK1) in the second order accurate single-step modified Euler (RK2). Hence, the RK12 uses the approximations computed from RK1 to compute second order accurate approximations. The estimate of the local truncation error *REL* is then computed from the difference between the two solutions of different order (see Equation 7). Inspection of Table 1 shows that the number of stages *s* of the RK12 is two meaning that two evaluations of the constitutive relations are required in each substep. As discussed later, this aspect is relevant here because it plays a role in the overall computational cost of the substepping scheme.

Table 1. Coefficients for the 2nd order Runge-Kutta with substepping (RK12) (Sloan et al., 2001)

s	a_{ik}					$\hat{b}_i$ (2nd)	b_i (1st)
1						1/2	1
2	1					1/2	0

Tables 2 and 3 summarise the coefficients b_i and a_{ik} for the third (RK23) and fourth (RK34) order Runge-Kutta substepping schemes, respectively. Full details of the derivation of these two integration schemes can be found in Fehlberg (1969, 1970). In contrast with RK12 (Table 1), the number of stages is three for the RK23 and five for the RK34 (see Table 2 and 3, respectively).

Table 2. Coefficients for the 3rd order Runge-Kutta with substepping (RK23) (Fehlberg, 1969)

s	a_{ik}					$\hat{b}_i$ (3rd)	b_i (2nd)
1						1/6	1/2
2	1					1/6	1/2
3	1/4	1/4				2/3	0

Table 3. Coefficients for the 4th order Runge-Kutta with substepping (RK34) (Fehlberg, 1969)

s	a_{ik}					$\hat{b}_i$ (4th)	b_i (3rd)
1						43/288	1/6
2	1/4					0	0
3	4/81	32/81				243/416	27/52
4	57/98	-432/343	1053/686			343/1872	49/156
5	1/6	0	27/52	49/156		1/12	0

The coefficients of the fifth order Runge-Kutta scheme with substepping (RK45) correspond to the family of higher order Runge-Kutta-Dormand-Prince methods proposed in Dormand & Prince (1980) and are summarised in Table 4. As discussed in Sloan et al. (2001), the RK45 scheme results in very accurate values for $\boldsymbol{\sigma}_n'$ and p'_{0n} at the end of each step/substep at the expense of additional evaluations of the constitutive relations (i.e. six stages, see Table 4). This method is hence useful for obtaining reference solutions to study the accuracy of a numerical scheme, but its implementation is considerably more tedious than the lower order schemes RK12 and RK23.

Table 4. Coefficients for the 5th order Runge-Kutta with substepping (RK45) (Dormand & Prince, 1980)

s	a_{ik}					$\hat{b}_i$ (5th)	b_i (4th)
1						19/216	31/540
2	1/5					0	0
3	3/40	9/40				1000/2079	190/297
4	3/10	-9/10	6/5			-125/216	-145/108
5	226/729	-25/27	880/729	55/729		81/88	351/220
6	-181/270	5/2	-266/297	-91/27	189/55	5/56	1/20

4. IMPLICIT INTEGRATION SCHEMES

This section summarises the first order fully implicit backward Euler (BE1) integration scheme used to solve Equation 1. Further details on implicit algorithms can be found elsewhere (e.g. Simo & Taylor (1986), Jeremic & Sture (1997)).

Similar to the explicit schemes discussed earlier, it is useful to express Equation 1 in terms of a pseudo-time T so that the integration of the strain increment goes from $T = 0$ to $T = 1$ (or, more generally, from $T_{n\text{-}1}$ to T_n). The IVP defined by Equation 2 can be also integrated implicitly over T when knowing the initial state of the soil at n-1 (i.e. quantities $\boldsymbol{\sigma}'_{n\text{-}1}$ and $p'_{0n\text{-}1}$) and the imposed increment of strain $\Delta\boldsymbol{\varepsilon}$. The problem to be solved can be written as:

$$\begin{cases} \boldsymbol{\sigma}'_n + \Delta\lambda \mathbf{D}_e \mathbf{b} = \boldsymbol{\sigma}'_{n-1} + \mathbf{D}_e \Delta\boldsymbol{\varepsilon} \\ p'_{0n} - \Delta\lambda B = p'_{0n-1} \\ F\left(\boldsymbol{\sigma}'_n, p'_{0n}\right) = 0 \end{cases} \tag{13}$$

where F is the yield curve of the MCC evaluated at n.

The unknowns $\mathbf{x}$ in Equation 13 are:

$$\mathbf{x} = \begin{pmatrix} \boldsymbol{\sigma}'_n \\ p'_{0n} \\ \Delta\lambda \end{pmatrix} \tag{14}$$

and the residuals $\mathbf{r}$:

$$\mathbf{r} = \begin{pmatrix} \boldsymbol{\sigma}'_n + \Delta\lambda \mathbf{D}_e \mathbf{b} - \mathbf{D}_e \Delta\boldsymbol{\varepsilon} - \boldsymbol{\sigma}'_{n-1} \\ p'_{0n} - \Delta\lambda B - p'_{0n-1} \\ F\left(\boldsymbol{\sigma}'_n, p'_{0n}\right) \end{pmatrix} \tag{15}$$

In order to solve this nonlinear problem, the residuals in Equation 15 are minimised with an iterative method. The most common one is the Newton-Raphson method (NR) for which the jacobian matrix of the residuals is needed. The jacobian of this problem $\mathbf{J}$ can be easily formed by finding the derivatives of the residuals with respect to the unknowns:

$$\mathbf{J} = \begin{pmatrix} \mathbf{I}_{\sigma'} - \Delta\lambda \mathbf{D}_e \dfrac{\partial \mathbf{b}}{\partial \boldsymbol{\sigma}'} & \Delta\lambda \mathbf{D}_e \dfrac{\partial \mathbf{b}}{\partial p'_0} & \mathbf{D}_e \mathbf{b} \\ -\Delta\lambda \dfrac{\partial B}{\partial \boldsymbol{\sigma}'} & 1 - \Delta\lambda \dfrac{\partial B}{\partial p'_0} & -B \\ \mathbf{a}^T & \dfrac{\partial F}{\partial p'_0} & 0 \end{pmatrix} \tag{16}$$

where **a** is the derivative of the yield curve with respect to effective stress, A and B are the two scalar functions introduced earlier and $\mathbf{I}_x$ is the identity matrix of order $_x$ (see Pérez-Foguet et al. (2001ab) for more details).

The iterative increment of the unknowns is given by:

$$\delta\mathbf{x} = -\mathbf{J}^{-1}\mathbf{r} \tag{17}$$

With starting conditions corresponding to the elastic trial state (i.e. $\boldsymbol{\sigma}'_0 = \boldsymbol{\sigma}'_{n-1} + \mathbf{D}_e\Delta\boldsymbol{\varepsilon}$, $(p'_0)_0 = p'_{0n-1}$ and $\Delta\lambda_0=0$).

The iterations of the NR progress until the residuals converge within a given tolerance. Throughout the iteration process all derivatives are evaluated at the current state. Equation 13 is expressed in terms of effective stresses to ease the comparison with the explicit integration schemes presented previously. However, it can be also expressed in terms of strains (e.g. Coombs et al., 2010, 2011; Pedroso & Farias, 2005).

5. VERIFICATION AND COMPUTATIONAL ASPECTS

Although it is possible to formulate a substepping scheme in terms of *absolute* error (Lloret-Cabot et al., 2017b), the work presented here concentrates on the *relative* error. It is useful to distinguish two types of relative error in this section: the *local* relative error and the *cumulative* relative error. The local relative error is the error incurred by the numerical scheme in the integration of a single substep and will be indicated as e. In contrast, the accumulation of local relative error over a number of substeps is the cumulative relative error (sometimes also referred to as *global* relative error) and will be indicated as E.

A key aspect to check after the implementation of a substepping integration scheme is that the relative error incurred in the integrated variables of the model behaves as expected, firstly in a single substep (i.e. local relative error *e*) and subsequently over many substeps (i.e. cumulative relative error *E*). Hence, this section studies first the behaviour of *e* (i.e. *STOL* = 1). Different values of *STOL* are imposed subsequently to investigate the behaviour of *E*.

Two numerical tests are considered to study the behaviour of *e* and *E*. Both tests assume axisymmetric conditions and consider an initial stress state on the yield curve (at zero deviatoric stress) so that any increase in effective stress produces plastic yielding. Similar outcomes are expected for more general situations involving elasto-plastic transitions provided that the elastic incremental relations of the constitutive model are also integrated using the same substepping strategy used for plastic yielding and provided also that the solution of the intersection problem corresponds to that obtained from the higher order scheme.

The first of the numerical tests considered (Test A) studies the variation of the error for given finite equal variations of axial strain and radial strain $\Delta\varepsilon_a = \Delta\varepsilon_r \approx \Delta\varepsilon_v/3$. The second test considered (Test B) studies the error response for an axial strain increment $\Delta\varepsilon_a$ (with no radial strains, $\Delta\varepsilon_r$). The MCC constants and initial state considered in both tests are indicated in Table 5. The tolerance associated with the yield surface *FTOL* is 10^{-12} (and is the same value of tolerance used in the iterative NR method of the implicit backward Euler integration scheme).

Table 5. Values of soil constants and initial state for the MCC simulations for Tests A and B

$\lambda = 0.12$	$\kappa = 0.05$	$N = 2.00$	$p' = 50$ kPa
$\upsilon = 0.33$ (*)	$M = 1.20$	$q = 0$ kPa	$p_0' = 50$ kPa

(*) Poisson's ratio.

Test A is useful because it is trivial to find an analytical solution and hence the computation of the relative local error is exact. Test B, in contrast, uses a reference solution to compute the error which corresponds to the solution from the RK45 with *FTOL* = 10^{-13} and *STOL* = 10^{-13}. In both tests, the size of the increment of strain is

varied to study its influence in the solution. For Test A, $\Delta\varepsilon_v = 10^{-06}$ to 0.1 and for Test B, $\Delta\varepsilon_a = 10^{-06}$ to 0.1 (keeping $\Delta\varepsilon_r = 0$).

5.1. Single-step analysis: the relative local error *e*

The integrated variables in the integration schemes presented earlier are the effective stress $\boldsymbol{\sigma}'$ and mechanical hardening parameter p_0'. The local relative error in these variables (for a given strain increment) can be computed by comparing the numerical solution obtained from a particular integration scheme against a reference (or when possible analytical) solution, according to:

$$e_{\boldsymbol{\sigma}'} = \frac{\left\{\left(\boldsymbol{\sigma}'_{ref} - \boldsymbol{\sigma}'\right)^T \left(\boldsymbol{\sigma}'_{ref} - \boldsymbol{\sigma}'\right)\right\}^{1/2}}{\left\{\left(\boldsymbol{\sigma}'_{ref}\right)^T \left(\boldsymbol{\sigma}'_{ref}\right)\right\}^{1/2}} \tag{18}$$

$$e_{p'_0} = \frac{\left|p'_{0ref} - p'_0\right|}{p'_{0ref}} \tag{19}$$

where the subscript *ref* indicates a reference (or analytical) solution.

Local accuracy in each numerical method is assessed by plotting the local error in $\boldsymbol{\sigma}'$ and p_0' against the size of the increment of strain. All plots use logarithmic scales in both axes to verify that the gradient obtained for the best-fitted straight line through a particular set of error results corresponds to the theoretical order of accuracy of the integration scheme used.

Typical results of the behaviour of the local error in effective stresses and hardening parameter during the numerical integration of Test B are summarised in Tables 6 and 7, respectively, all using *STOL* = 1 (similar error responses are obtained for the simpler Test A, see Appendix). Inspection of these tables show that the overall behaviour is as expected, with errors in $\boldsymbol{\sigma}'$ and p_0' decreasing with the decrease of the axial strain size. Such decrease in error is greater in the integration schemes with higher order of accuracy. As illustrated later in Figure 1, the error results for the explicit single-step 1st order forward Euler (RK1) and for the implicit single-step 1st order backward Euler (BE1) are similar for all strain increment sizes considered. However, the values of *e* in

the BE1 are always smaller (when compared against the corresponding values from RK1) but these are of several order of magnitude greater than the typical accuracy achieved by the other higher order explicit schemes (see Tables 6 and 7).

Table 6. Local relative error values in effective stress **σ'** for a single elasto-plastic axial straining step considering *STOL* = 1 and keeping $\Delta\varepsilon_r = 0$ (Test B).

	Explicit					Implicit
$\Delta\varepsilon_a$	1st order (RK1)	2nd order (RK2)	3rd order (RK3)	4th order (RK4)	5th order (RK5)	1st order (BE1)
$1\cdot10^{-06}$	$1.75\cdot10^{-10}$	$3.25\cdot10^{-15}$	$< 1.0\cdot10^{-15}$	$< 1.0\cdot10^{-15}$	$< 1.0\cdot10^{-15}$	$7.32\cdot10^{-11}$
$1\cdot10^{-05}$	$1.75\cdot10^{-08}$	$2.98\cdot10^{-12}$	$1.15\cdot10^{-15}$	$1.15\cdot10^{-15}$	$< 1.0\cdot10^{-15}$	$7.32\cdot10^{-09}$
$1\cdot10^{-04}$	$1.74\cdot10^{-06}$	$2.99\cdot10^{-09}$	$9.40\cdot10^{-12}$	$1.15\cdot10^{-15}$	$< 1.0\cdot10^{-15}$	$7.31\cdot10^{-07}$
$1\cdot10^{-03}$	$1.68\cdot10^{-04}$	$3.01\cdot10^{-06}$	$9.07\cdot10^{-08}$	$1.43\cdot10^{-10}$	$1.72\cdot10^{-12}$	$7.17\cdot10^{-05}$
$1\cdot10^{-02}$	$1.19\cdot10^{-02}$	$2.78\cdot10^{-03}$	$6.01\cdot10^{-04}$	$6.85\cdot10^{-06}$	$1.06\cdot10^{-06}$	$5.56\cdot10^{-03}$
$1\cdot10^{-01}$	$2.81\cdot10^{-01}$	$1.36\cdot10^{-01}$	$1.83\cdot10^{-01}$	$2.83\cdot10^{-02}$	$3.86\cdot10^{-02}$	$2.11\cdot10^{-01}$

Table 7. Local relative error values in the mechanical hardening parameter p_0' for a single elasto-plastic axial straining considering *STOL* = 1 and keeping $\Delta\varepsilon_r = 0$ (Test B).

	Explicit					Implicit
$\Delta\varepsilon_a$	1st order (RK1)	2nd order (RK2)	3rd order (RK3)	4th order (RK4)	5th order (RK5)	1st order (BE1)
$1\cdot10^{-06}$	$2.34\cdot10^{-10}$	$3.98\cdot10^{-15}$	$< 1.0\cdot10^{-15}$	$< 1.0\cdot10^{-15}$	$< 1.0\cdot10^{-15}$	$1.91\cdot10^{-11}$
$1\cdot10^{-05}$	$2.34\cdot10^{-08}$	$2.38\cdot10^{-12}$	$< 1.0\cdot10^{-15}$	$< 1.0\cdot10^{-15}$	$< 1.0\cdot10^{-15}$	$1.91\cdot10^{-09}$
$1\cdot10^{-04}$	$2.34\cdot10^{-06}$	$2.39\cdot10^{-09}$	$7.41\cdot10^{-12}$	$< 1.0\cdot10^{-15}$	$< 1.0\cdot10^{-15}$	$1.89\cdot10^{-07}$
$1\cdot10^{-03}$	$2.27\cdot10^{-04}$	$2.46\cdot10^{-06}$	$7.07\cdot10^{-08}$	$5.44\cdot10^{-11}$	$1.04\cdot10^{-12}$	$1.72\cdot10^{-05}$
$1\cdot10^{-02}$	$1.71\cdot10^{-02}$	$2.52\cdot10^{-03}$	$4.19\cdot10^{-04}$	$1.91\cdot10^{-06}$	$1.91\cdot10^{-06}$	$8.70\cdot10^{-04}$
$1\cdot10^{-01}$	$2.88\cdot10^{-01}$	$1.36\cdot10^{-01}$	$1.27\cdot10^{-01}$	$3.16\cdot10^{-03}$	$2.95\cdot10^{-02}$	$2.22\cdot10^{-01}$

Figure 1 illustrates the local relative error for Test B in terms of effective stress (Figure 1a) and mechanical hardening parameter (Figure 1b). Symbols indicate the computed relative error and each dashed line indicates the best-fitted straight line through the computed local relative error from results a particular numerical method. These dashed lines are referred to hereafter as *local error lines*.

Assuming no cancellation, the expression of a local error line in terms of the substep size *h* can be written as:

$$e \approx ch^{p+1} \tag{20}$$

where *p* is the order of the integration scheme and *c* is a constant.

Equation 20 indicates that the local error line of a substepping scheme of order p will have a gradient of $p + 1$ when plotting the local relative error e against the step size h. This information is included in Figure 1 to demonstrate that the six single-step integrations involved are performing correctly. Although not plotted, similar numerical outcomes are obtained for the simpler numerical Test A (see Appendix).

Inspection of Figure 1 confirms the previous discussion on the similar accuracy achieved by RK1 and BE1, and the larger differences in accuracy observed in the local error values from the higher order schemes. Interestingly, for the largest increment size (i.e. $\Delta\varepsilon_a = 10^{-01}$), all methods reach a similar value of local relative error indicating that this strain increment size is too large to show differences in accuracy between methods and, hence, suggesting that smaller increment sizes should be used for this problem.

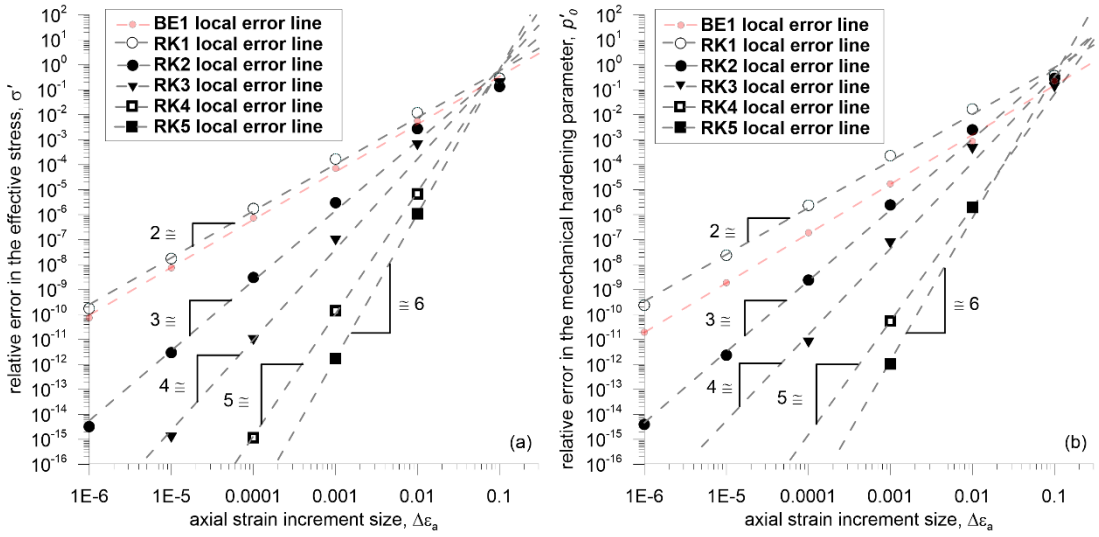

Figure 1. Local relative error against axial strain increment size for a single elasto-plastic axial strain increment at constant radial strain (Test B): (a) effective stress **σ'**; (b) mechanical hardening parameter p_0'. BE1, 1st order single-step backward Euler; RK1, 1st order single-step Runge-Kutta; RK2, 2nd order single-step Runge-Kutta; RK3, 3rd order single-step Runge-Kutta; RK4, 4th order single-step Runge-Kutta; RK5, 5th order single-step Runge-Kutta.

5.2. Substepping analysis: the cumulative relative error *E*

After checking that integration at a single-step performs correctly, the verification of the numerical performance of the explicit substepping schemes over several substeps

must be then checked. As suggested in Lloret-Cabot et al. (2016), this can be studied by looking at the behaviour of the cumulative relative error E when the substepping is active.

Assuming n equal-sized substeps of size h, the cumulative relative error can be expressed as:

$$E \approx nch^{p+1} = Hch^{p} \tag{21}$$

where H is the size of the total increment integrated i.e. $H=hn$.

Equation 21 indicates that the final cumulative relative error (incurred during the integration of a given total increment H) approximately lies on a straight line when plotted against the substep size h in a log-log scale, having gradient 2 for the RK12, 3 for RK23, 4 for the RK34 and 5 for RK45 (note that the BE1 is a single-step method so the terms local and cumulative error are equivalent). Hence, similarly to the local error lines plotted in Figure 1 for a single-step/substep, Equation 21 defines another error line of gradient p that will be referred to hereafter as *cumulative error line*. An interesting well-known implication from this is that the error in a substepping integration scheme is controlled by the error in the approximations of the lower order scheme (Sloan et al., 2001). Indeed, according to Equation 7, the substepping schemes considered here estimate the local truncation error (*REL*) as the difference between the numerical approximations of $\boldsymbol{\sigma}'$ and p_0' obtained from the lower order scheme and those obtained from the higher order scheme (and dividing this difference by the corresponding higher order approximation). Given that the approximations from the lower order scheme are the largest source of error, the order of accuracy of this difference is controlled by the lower order scheme. For example, in the RK12, this difference has order $p = 1$ which, as illustrated in Figure 2, corresponds to a straight line of gradient $p + 1 = 2$ when plotting the computed values of *REL* in terms of the increment size of strain in the log-log scale. Similar results are observed for RK23, RK34 and RK45 (Figure 2).

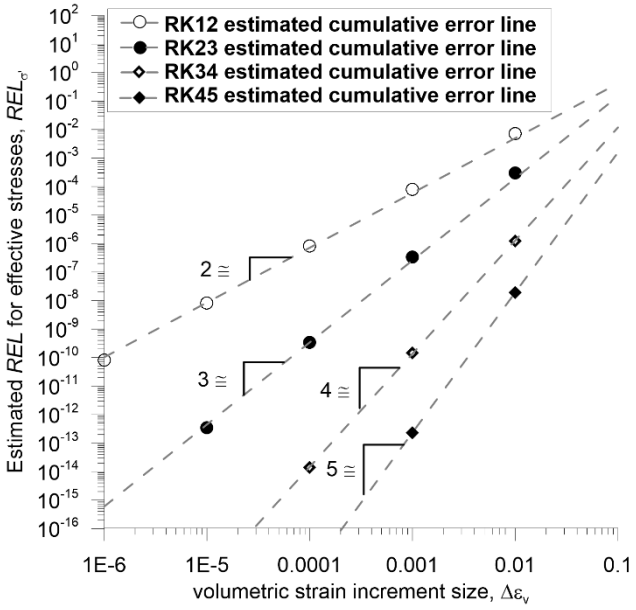

367

368 Figure 2. Estimate of the local truncation error *REL* for effective stresses against
369 volumetric strain increment size for a single elasto-plastic volumetric strain increment
370 (Test A). RK12, 2nd order Runge-Kutta with substepping; RK23, 3rd order Runge-Kutta
371 with substepping; RK34, 4th order Runge-Kutta with substepping; RK45, 5th order
372 Runge-Kutta with substepping.

373 Once the local truncation error is estimated, the substepping scheme decides the size of
374 the substep at which the integration will proceed. Such decision is done by comparing
375 the imposed value of *STOL* against the maximum value of *REL* computed using
376 Equation 7. If *REL* > *STOL*, the substep fails and the algorithm reduces the size of the
377 substep according to Equation 9, 10, 11 or 12 (depending on the substepping scheme
378 used). The same check is then carried out with the new value of *REL* computed with
379 the adjusted substep size. If *STOL* ≤ *REL*, the substepping algorithm advances in the
380 solution with the current substep size.

381 This process is illustrated in Figure 3 for the RK12 (Figure 3a), RK23 (Figure 3b),
382 RK34 (Figure 3c) and RK45 (Figure 3d) when solving the numerical Test A with an
383 initial increment of volumetric strain $\Delta\varepsilon_v = 0.1$ and $STOL = 10^{-08}$. The error line
384 corresponding to the single-step implicit backward Euler has also been included in these
385 plots for comparison.

386 In all four plots, the intersection of the horizontal thicker dashed line (indicating the
387 value of the imposed *STOL*) with the local error line of the lower order method (for a

particular substepping scheme) gives the approximate optimal substep size at which the algorithm advances the integration. For example, in Figure 3a, this intersection occurs at a substep size of $\delta\varepsilon_v \approx 10^{-5}$ (as indicated by the arrow). This means that in the RK12, the initial volumetric strain size has to be reduced by almost 10,000 times to satisfy the requirement imposed by $STOL = 10^{-8}$. In contrast, a reduction of about 400 times is required in the RK23, 40 in the RK34 and 10 in the the RK45. These quantities are relevant here because the smaller the substep size, the larger will be the number of substeps required to integrate the full increment $\Delta\varepsilon_v = 0.1$ (which, in turn, will increase the computational cost). Note that, as further investigated later, the overall computational cost needs to account also for the number of evaluations of the constitutive relations which differs between substepping schemes (see Tables 1 to 4).

As demonstrated previously, the local error for the first integrated substep of size $\delta\varepsilon_v$ (if integrated correctly) should lie on the local error line of the substepping scheme corresponding to the higher order integration (because local extrapolation is used). For example, the local error line for the RK12 is $e \approx ch^3$ and the local error for the first substep size $\delta\varepsilon_v \approx 1.1 \cdot 10^{-5}$ is of about $e \approx 4 \cdot 10^{-13}$ which, in fact, lies on an error line of gradient 3 (Figure 3a). Equivalent results are found for the other integration schemes plotted in Figure 3.

The local error incurred in the integration of subsequent substeps is accumulated as the solution advances and, when the substeps integrated are of similar size, such accumulation of error results in an approximately vertical line when plotted in the ln$e$:ln$h$ plane (see Figure 3) confirming the assumption made in deriving Equation 21. Closer inspection of Figure 3a shows that the cumulative error in integrating the complete $\Delta\varepsilon_v = 0.1$ with $STOL=10^{-08}$ when using the RK12 is about $E \approx 3.6 \cdot 10^{-09}$ and is bounded by the local error line corresponding to the embedded 1st order Euler scheme (which, as expected, is parallel to the BE1 error line, see Figure 3a). It is important to realise here that the cumulative error incurred by BE1 in integrating the complete $\Delta\varepsilon_v = 0.1$ is instead several orders of magnitude greater $e = E \approx 2.16 \cdot 10^{-01}$ (because no substepping is involved). This difference in accuracy is even more noticeable when comparing BE1 results against higher order accurate substepping schemes, in agreement with the findings of Pedroso & Farias (2005) and Potts & Ganendra (1994). However, the observed improvement in accuracy of the explicit substepping schemes

is at the expense of a larger computational cost: while only few NR iterations are needed in the BE1 to integrate $\Delta\varepsilon_v = 0.1$, about 10,000 substeps are required in the RK12.

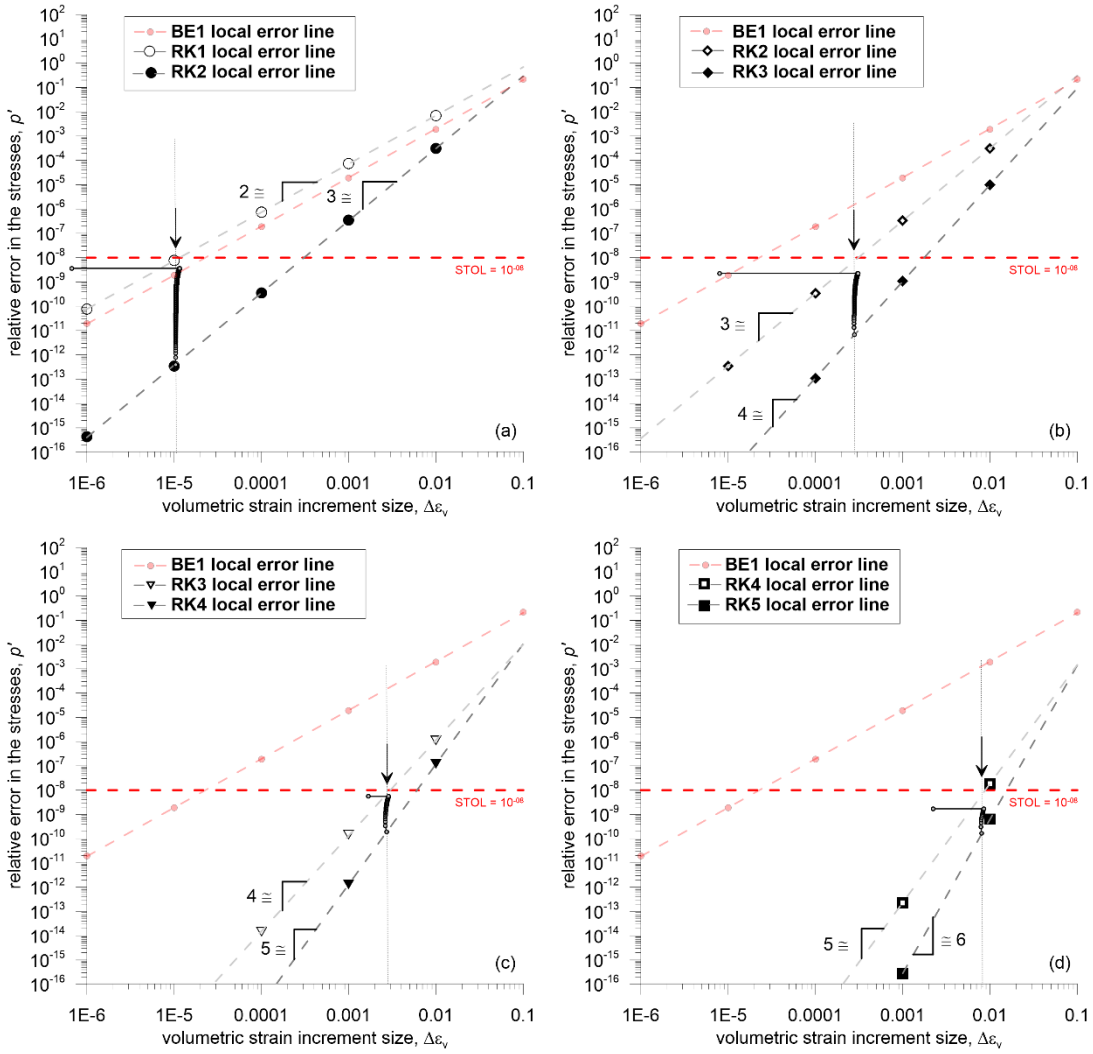

Figure 3. Relative error in mean effective stress *p*' against volumetric strain increment size for a single elasto-plastic isotropic strain increment (Test A): (a) 2nd order Runge-Kutta with substepping (RK12); (b) 3rd order Runge-Kutta with substepping (RK23); (c) 4th order Runge-Kutta with substepping (RK34); (d) 5th order Runge-Kutta with substepping (RK45).

An expanded version of Figure 3 including different *STOLs* is presented in Figures 4, 5, 6 and 7 for the RK12, RK23, RK34 and RK45 respectively. In all figures, the values of *STOL* vary from 1 to 10^{-08} and the strain increment assumed is $\Delta\varepsilon_v = 0.1$ (Test A). The corresponding cumulative error results are presented in Table 8 which includes the cumulative error in BE1 approximations, for completeness. The total number of

substeps (TS) and the total number of failed substeps (TF) required in all four explicit substepping integration schemes considered is presented in Table 9 (no drift correction iterations were necessary). For completeness, the number of NR iterations for the BE1 is also included in Table 9.

Table 8. Typical cumulative relative error values E in effective stress $\boldsymbol{\sigma}'$ for an elasto-plastic isotropic strain increment of $\Delta\varepsilon_v = 0.1$ (Test A) considering different values of *STOL*.

Implicit	Explicit				
E in 1st order (BE1)	*STOL*	E in 2nd order (RK12)	E in 3rd order (RK23)	E in 4th order (RK34)	E in 5th order (RK45)
$2.16\cdot10^{-01}$	1	$1.23\cdot10^{-01}$	$3.51\cdot10^{-02}$	$4.69\cdot10^{-03}$	$3.92\cdot10^{-04}$
	$1\cdot10^{-02}$	$3.52\cdot10^{-03}$	$2.40\cdot10^{-03}$	$4.69\cdot10^{-03}$	$3.92\cdot10^{-04}$
	$1\cdot10^{-04}$	$3.58\cdot10^{-05}$	$2.17\cdot10^{-05}$	$7.84\cdot10^{-05}$	$4.46\cdot10^{-05}$
	$1\cdot10^{-06}$	$3.58\cdot10^{-07}$	$2.22\cdot10^{-07}$	$5.78\cdot10^{-07}$	$1.99\cdot10^{-07}$
	$1\cdot10^{-08}$	$3.58\cdot10^{-09}$	$2.23\cdot10^{-09}$	$5.56\cdot10^{-09}$	$1.71\cdot10^{-09}$

Table 9. Total number of Newton-Raphson (NR) iterations required by the BE1 together with the total number of substeps (TS) and total number of failed substeps (TF) required by the explicit integration schemes to integrate an elasto-plastic isotropic strain increment of $\Delta\varepsilon_v = 0.1$ (Test A) considering different values of *STOL*.

Implicit	Explicit								
1st order (BE1)	*STOL*	2nd order (RK12)		3rd order (RK23)		4th order (RK34)		5th order (RK45)	
NR iterations		TS	TF	TS	TF	TS	TF	TS	TF
12	1	1	0	1	0	1	0	1	0
	$1\cdot10^{-02}$	9	2	4	2	1	0	1	0
	$1\cdot10^{-04}$	91	2	16	2	4	2	2	2
	$1\cdot10^{-06}$	910	3	74	2	12	2	5	2
	$1\cdot10^{-08}$	9105	4	344	3	37	2	13	2

Inspection of Tables 8 and 9 show how the cumulative error behaves during the elasto-plastic integration of the entire $\Delta\varepsilon_v$. For single substep integration (*STOL* = 1) the error values are quite large and are similar in the lower order schemes (i.e. BE1, RK12 and RK23), which seems to confirm that $\Delta\varepsilon_v = 0.1$ is too large to be integrated in one step with these schemes. When the substepping is active, lower values of cumulative error are observed if reducing values of *STOL* (Table 8), but these involve a larger number of substeps (Table 9). Closer inspection of Table 8 shows that for a given value of *STOL* the values of cumulative error are of the same order of magnitude in all four substepping

schemes, with slightly lower values of E being typically observed for higher order schemes (except for RK34 where the values of E are slightly greater than those of RK23). The important difference to note in Tables 8 and 9 is that the optimal substep size employed in each integration scheme for a given *STOL* is different and, hence, the number of substeps needed to integrate the full increment is also different. In general, larger substep sizes can be used with higher order methods without compromising the accuracy. As a consequence, a lower number of substeps is required in the higher order methods (Table 9).

Similar comments are valid for Figures 4 to 7. In all cases, the final values of cumulative relative error (once the entire $\Delta\varepsilon_v$ has been integrated) lie on a cumulative error line with a gradient corresponding to the lower order embedded scheme. For example, for the RK12, all final values of E lie on a straight line of gradient 2 (see short dashed dotted line in Figure 4) which is parallel to the first order single-step methods. Note that other parallel cumulative error lines exist for smaller increments of strains but are not included here for clarity.

Lloret-Cabot et al. (2016) show that the number of substeps required to integrate the entire $\Delta\varepsilon_v$ for a given substep size h can also be checked because $e/E \approx h/H \approx 1/n$ where n is the number of substeps required to integrate the full increment H. This aspect can be easily verified here by ensuring that the total number of substeps indicated in Table 9 for a particular substepping scheme corresponds to the expected value. For example, the substep size required in the RK12 to integrate the entire increment $\Delta\varepsilon_v = 0.1$ with $STOL = 10^{-08}$ is about $\delta\varepsilon_v \approx 1.1 \cdot 10^{-5}$ (see Figure 4) which means that the total number of substeps required to integrate the full increment is approximately $n \approx \Delta\varepsilon_v/\delta\varepsilon_v = 9{,}090$ which is very close to the actual number of substeps used 9,105 (see Table 9).

The BE1 error line is also included in the figures for comparison. Interestingly, this line is almost coincident with the cumulative error line for the RK12. The important thing to remind here is that the BE1 is a single-step scheme and, hence, the total size integrated corresponds to the value displayed in the horizontal axis. In contrast, the total size integrated for the RK12 is, in all cases, $\Delta\varepsilon_v = 0.1$ which requires using multiple substeps of size $\delta\varepsilon_v$ (and such substep size reduces when reducing *STOL*).

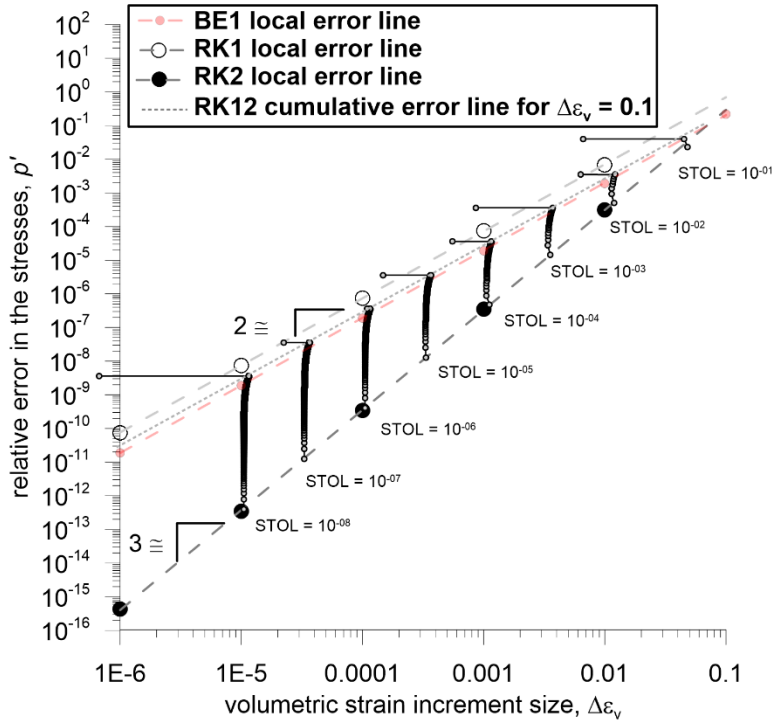

481

482 Figure 4. Cumulative relative error behaviour in effective stresses for the 2nd order
483 Runge-Kutta with substepping (RK12) against strain increment size for an elasto-
484 plastic isotropic strain increment (Test A). BE1, 1st order single-step backward Euler;
485 RK1, 1st order-single step Runge-Kutta; RK2, 2nd order single-step Runge-Kutta.

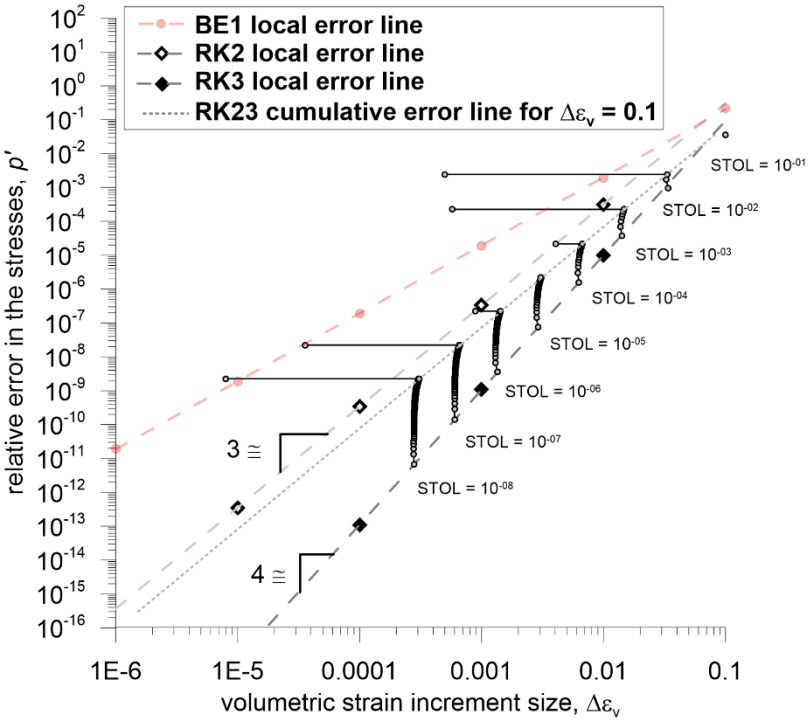

486

Figure 5. Cumulative relative error behaviour in effective stresses for the 3rd order Runge-Kutta with substepping (RK23) against strain increment size for an elasto-plastic isotropic strain increment (Test A). BE1, 1st order single-step backward Euler; RK2, 2nd order-single step Runge-Kutta; RK3, 3rd order single-step Runge-Kutta.

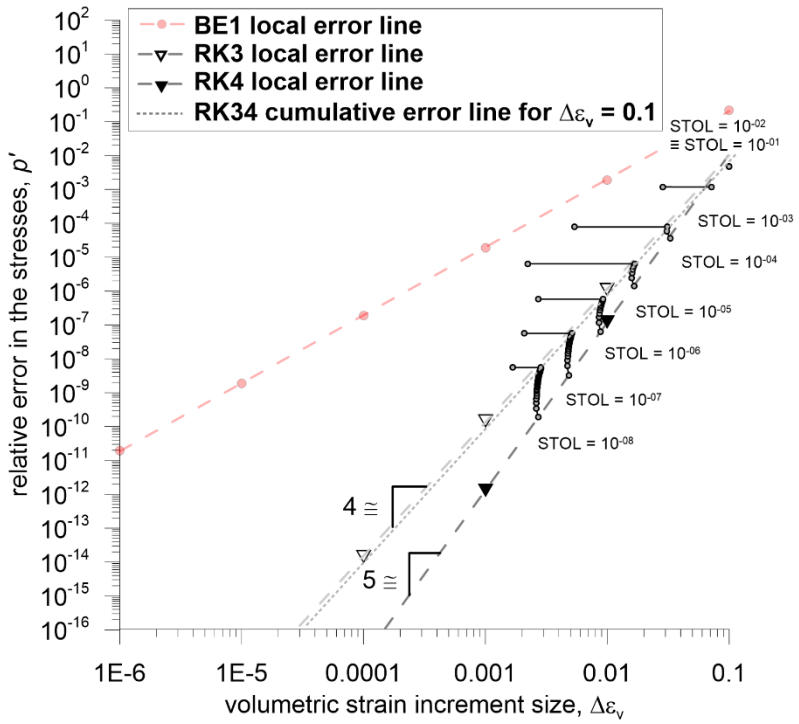

Figure 6. Cumulative relative error behaviour in effective stresses for the 4th order Runge-Kutta with substepping (RK34) against strain increment size for an elasto-plastic isotropic strain increment (Test A). BE1, 1st order single-step backward Euler; RK3, 3rd order-single step Runge-Kutta; RK4, 4th order single-step Runge-Kutta.

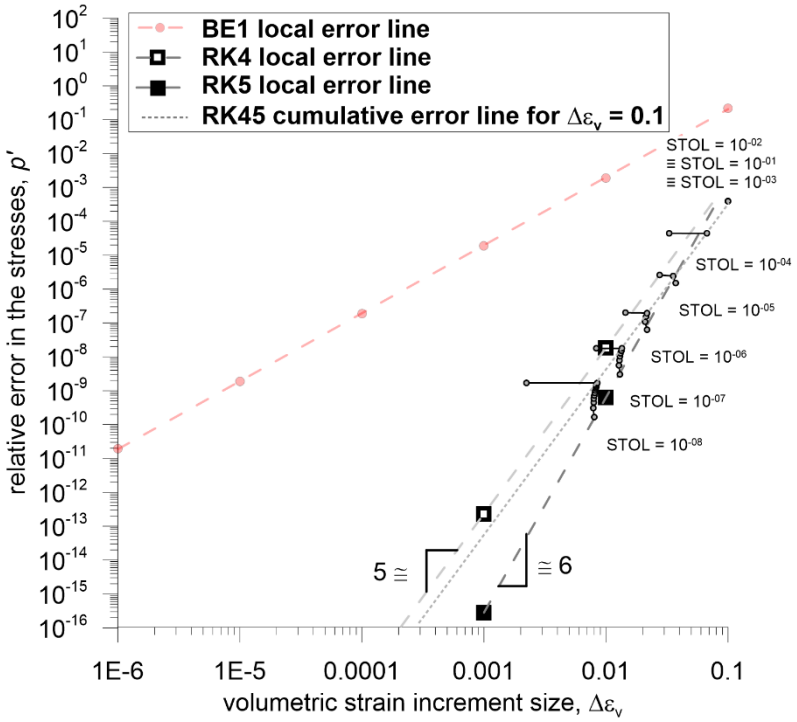

496

497 Figure 7. Cumulative relative error behaviour in effective stresses for the 5th order
498 Runge-Kutta with substepping (RK45) against strain increment size for an elasto-
499 plastic isotropic strain increment (Test A). BE1, 1st order single-step backward Euler;
500 RK4, 4th order-single step Runge-Kutta; RK5, 5th order single-step Runge-Kutta.

501 5.3 Performance maps

502 Lloret-Cabot et al. (2016) propose a form of plotting the computational outcomes from
503 a substepping integration scheme that is useful for a further comparison between the
504 four explicit substepping schemes investigated. This graphical form of presenting the
505 substepping results is referred to as the *performance maps* and includes two types of
506 plots. The first one represents the cumulative error against the number of substeps for
507 different increment sizes. The second represents the cumulative error against the value
508 of *STOL* for different increment sizes. For comparison, the results corresponding to the
509 fully implicit first other backward Euler for $\Delta\varepsilon_a = 10^{-06}$, 10^{-05}, 10^{-04}, 10^{-03}, 10^{-02} and 10^{-01} have been also included. Without loss of generality, the performance maps are only
511 presented here for Test B (similar results are obtained for the simpler Test A, see
512 Appendix).

Figure 8 illustrates how the number of substeps influences the cumulative relative error in the effective stress when integrating an axial strain increment $\Delta\varepsilon_a$ of a given size (equivalent results are obtained for the hardening parameter but not included for clarity). Inspection of Figure 8 shows that, as expected, when the number of substeps required to integrate a given increment size of axial strain increases (due to a more restrictive *STOL*) the value of cumulative error tends to decrease. The rate of such reduction is imposed by Equation 9, 10, 11 or 12, and it can be easily verified by plotting the error results of the corresponding integration scheme in the ln*E*:ln*n* plane (Figure 8). Note that the number of substeps for the BE1 is always one, but the cumulative error also increases with increasing $\Delta\varepsilon_a$ (see the vertical segment corresponding to error results from one single substep with each dot indicating a strain increment size). Given that BE1 is the scheme with the lowest order of accuracy, the value of *E* for a given size of $\Delta\varepsilon_a$ is always greater than the corresponding value of *E* obtained from any of the other schemes, and this is also true for *STOL*=1 (single-step integration).

Figure 9 illustrates the effect of varying *STOL* in the cumulative relative error in effective stresses when integrating a given axial strain increment $\Delta\varepsilon_a$. Obviously, this effect is only studied for the substepping schemes because the BE1 is a single-step integration scheme (equivalent to *STOL* = 1 in the substepping schemes).

As discussed earlier, reducing the value of *STOL* typically implies a reduction in the substep size $\delta\varepsilon_a$ which leads to a smaller value of the local relative error incurred in each individual substep of this size. A reduction in the cumulative error is hence also expected for lower *STOLs* once the full increment has been integrated (Figure 8). However, this reduction in the cumulative error with decreasing *STOL* is not always apparent in Figure 9 because, for the smaller sizes of axial strain, the substepping strategy is not always activated. The non-activation of the substepping strategy can be easily identified in Figure 9 by the constant (horizontal) variation of the cumulative error with *STOL* which indicates that the current substep size fulfils the restriction imposed by *STOL*. In contrast to these horizontal segments of the plot, a 1:1 gradient variation of the cumulative error with *STOL* is also observed in other parts of the plot indicating that substepping is active. This transition from no substepping to substepping is identified by a sharp change in the error behaviour (which, for the particular case of

$\Delta\varepsilon_a = 0.01$, has been indicated by point Y). Similarly to Figure 8, the error values for the BE1 result in a vertical segment at *STOL* = 1.

Comparing the four plots in Figure 8, it becomes apparent that there is a substantial computational gain with the order of the substepping scheme, especially in terms of efficiency. For example, to integrate an axial increment size of 0.01 with *STOL* = 10^{-08} only 5 substeps are required in the RK45 to reach an accuracy between 10^{-09}-10^{-10} (Figure 8d), 9 in the RK34 (Figure 8c), 68 substeps in the RK23 (Figure 8b) and 1,423 in the RK12 (Figure 8a) (note that the number of substeps *n* under discussion has been also included in Figure 9 for completeness). Furthermore, substepping is not even necessary in RK45 for values of *STOL* greater than 10^{-05}, in RK34 greater than 10^{-04}, in RK23 greater than 10^{-02} and in RK12 greater than 10^{-01}. These outcomes seem to suggest that the extra work required in the implementation of a higher order scheme might be worth the effort, especially for the RK23 as it only requires one more stage than RK12 (see Tables 1 and 2). To investigate this aspect further, it is necessary to assess the overall computational cost involved in integrating a given increment of strain, including not only the number of substeps (as discussed in Figures 8 and 9) but also the number of evaluations of the constitutive relations (and accounting for the number of failed substeps). For the BE1, on the other hand, the overall cost needs to account for the number of Newton-Raphson iterations used. This analysis is carried out in the next section.

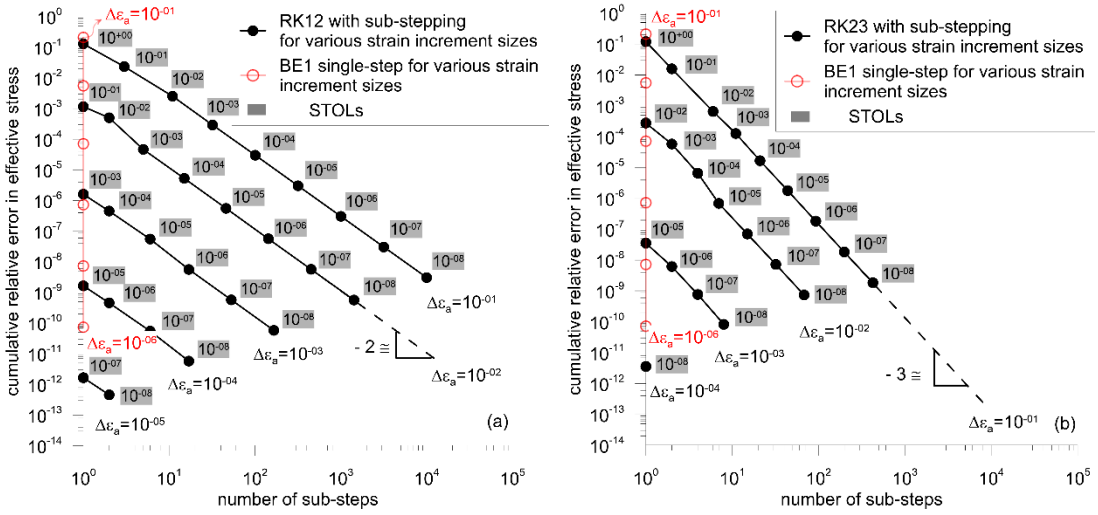

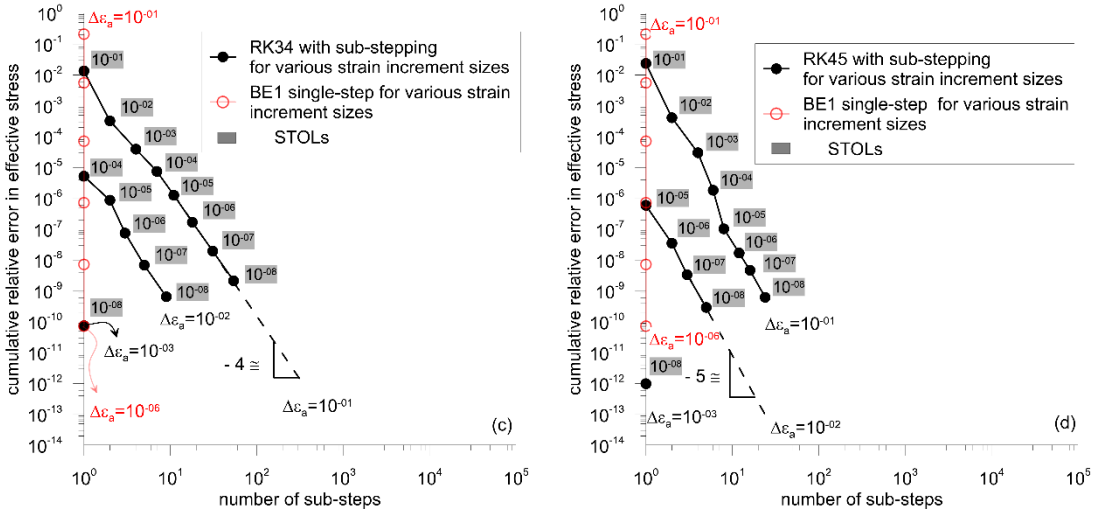

564 Figure 8. Cumulative relative error behaviour against number of substeps for an elasto-
565 plastic axial strain increment at constant radial strain (Test B): (a) 2nd order Runge-
566 Kutta with substepping (RK12); (b) 3rd order Runge-Kutta with substepping (RK23);
567 (c) 4th order Runge-Kutta with substepping (RK34); (d) 5th order Runge-Kutta with
568 substepping RK45. BE1, 1st order single-step backward Euler.

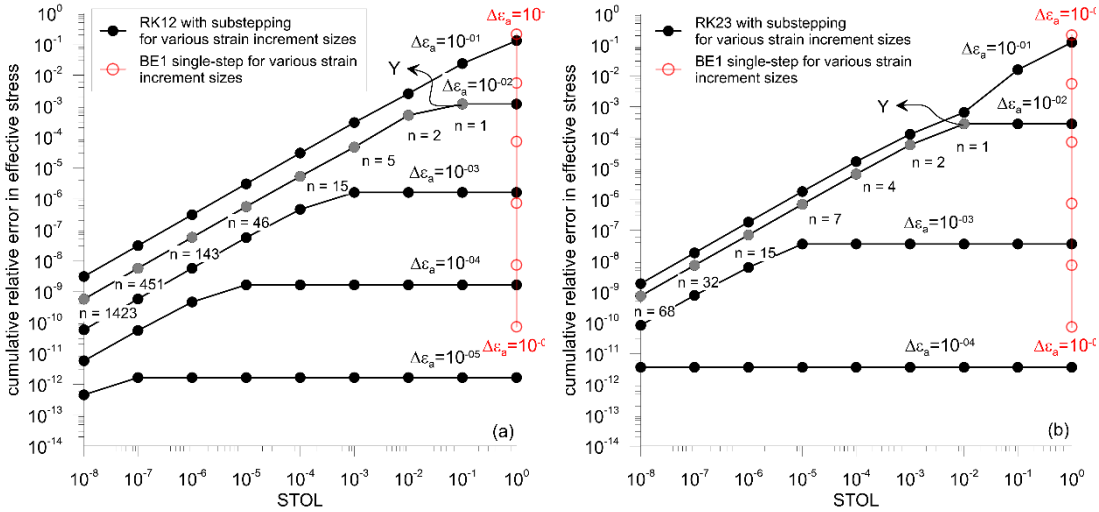

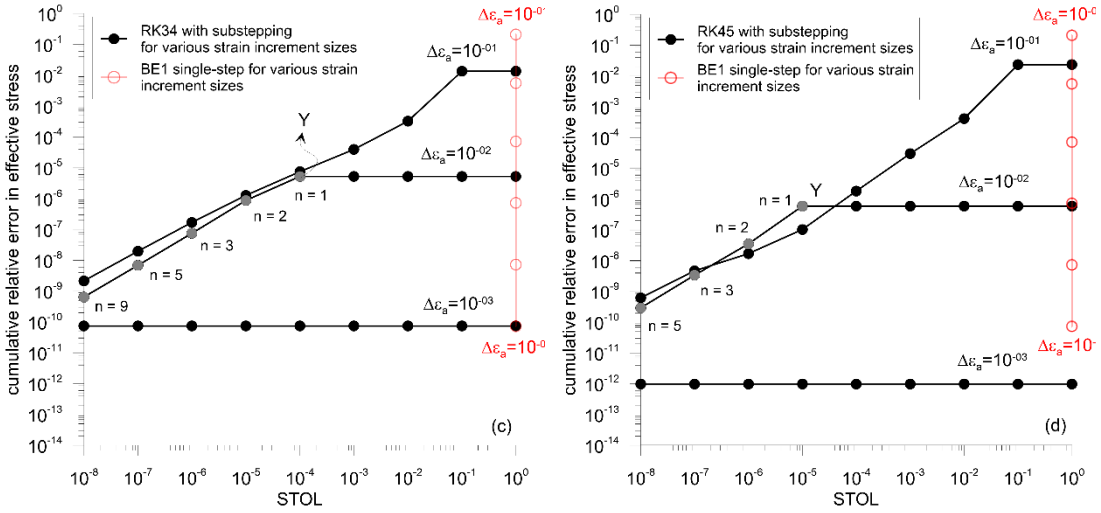

569 Figure 9. Cumulative relative error behaviour against *STOL* for an elasto-plastic axial
570 strain increment at constant radial strain (Test B): (a) 2nd order Runge-Kutta with
571 substepping (RK12); (b) 3rd order Runge-Kutta with substepping (RK23); (c) 4th order
572 Runge-Kutta with substepping (RK34); (d) 5th order Runge-Kutta with substepping
573 (RK45). BE1, 1st order single-step backward Euler.

574 5.4. Computational cost

575 This section aims at providing some further evidence on whether the extra work
576 required in implementing higher order schemes is worth the effort. For the discussion,
577 it is useful to compute the computational cost for solving Tests A and B with the BE1,
578 RK12, RK23, RK34 and RK45.

579 Due to their simplicity, a very small CPU time is associated with the solution of Tests
580 A and B. Hence, a common approach is to compute the computational cost
581 proportionally to the number of evaluations of the constitutive relations that each
582 substepping integration scheme employs in solving the problem (Sloan et al., 2001).
583 Two evaluations of the constitutive relations per substep are considered for the RK12,
584 three for the RK23, five for the RK34 and six for the RK45 (see the number of stages
585 of each scheme in Tables 1 to 4). Rejected substeps (as well as any iteration required in
586 the drift correction subroutine) also need to be accounted for. The number of
587 evaluations of the constitutive relations for the BE1 corresponds to the number of NR
588 iterations used to converge to the solution using a tolerance of 10^{-12}.

Figure 10 shows the computational cost as a function of the input increment size for the two numerical tests considered. Plots on the left correspond to results for Test A and plots on the right for Test B. To illustrate the influence of the substepping tolerance in the explicit schemes, different values of *STOL* (i.e. *STOL*= 10^{-02}, 10^{-04}, 10^{-06} and 10^{-08}) have been considered for the RK12, RK23, RK34 and RK45. In contrast, the single-step BE1 involves only one calculation.

The first part of the discussion compares the implicit BE1 against the explicit substepping schemes whereas the second part focusses on explicit substepping strategies alone. In order to make a fair comparison between implicit and explicit integration schemes, it is useful to consider the situation when no substepping is active so that the number of evaluations of the constitutive relations corresponds to the number of stages of the explicit RK substepping method. Against this background, the total computational cost for the BE1 involves between 3 and 12 NR iterations for Test A and between 4 and 18 NR iterations for Test B, depending on the increment size (see Figure 10). These values are generally higher than the stages required in the lower order RK12 and RK23 schemes when no substepping is active (i.e. 2 and 3 respectively), even though the level of accuracy achieved by these explicit substepping schemes is an order of magnitude higher. In contrast, a similar number of evaluations is involved in the higher order RK34 and RK45 schemes (when no substepping is active) requiring 5 and 6 stages, respectively (but, as discussed earlier, a much better accuracy is achieved by these). In summary, unlike differences in accuracy, differences in cost between schemes are very small when assuming single-step integration.

Once the substepping is active, the computational cost involved in the explicit schemes increases with *STOL* and this is especially true in the lower order substepping schemes (see Figure 10). Notably, for stringent values of *STOL* (*STOL* < 10^{-06}) and relatively large increment sizes ($\Delta\varepsilon_v$, $\Delta\varepsilon_a > 0.01$), the lower order substepping schemes RK12 and RK23 tend to spend more computational resources than those used by the BE1. This result, however, should be taken with caution because the accuracy achieved by the BE1 is significantly poorer, as discussed earlier (see Figures 8 and 9). Furthermore, the flexibility of the substepping schemes to vary the value of *STOL* is in fact a very useful feature as it allows for some control in the accuracy of the approximations (something not possible in the single-step BE1).

Focussing now only on the explicit substepping schemes, RK12 and RK23 require a larger number of evaluations of the constitutive relations (i.e. higher computational cost) to satisfy the value of *STOL* when the sizes of the input increment $\Delta\varepsilon_v$ or $\Delta\varepsilon_a$ are relatively large (i.e. $\Delta\varepsilon_v$, $\Delta\varepsilon_a > 0.001$), because of the larger number of substeps required. This observation is more obvious when the values of *STOL* become more restrictive. In contrast, RK34 and RK45 tend to be more expensive for the smaller increment sizes (i.e. $\Delta\varepsilon_v$, $\Delta\varepsilon_a < 0.001$). However, for smaller sizes, the number of evaluations is so small in all cases (i.e. less than 10) that differences between schemes in terms of computational cost are very small.

Comparison of the results for RK34 and RK45 shows very similar behaviour suggesting that the computational gain in implementing a RK45 method is not substantial in terms of cost and would only make sense if very accurate solutions are desired (see also Table 9). In contrast, a more substantial improvement is seen when comparing results for RK34 and RK23. For example, for an increment size of axial strain $\Delta\varepsilon_a = 0.01$ with $STOL = 10^{-06}$, the RK34 requires 3 evaluations, whereas for the same conditions, the RK23 needs 15. These differences between RK34 and RK23 become slightly more apparent for more demanding values of *STOL*. It is important to highlight, however, that the effort in implementing a RK34 scheme (when compared with that required to implement a RK23 scheme) is considerable, as the former involves 5 stages whereas the latter only three (see Tables 3 and 2, respectively).

The most interesting comparison between substepping schemes is perhaps with RK12 and RK23, because the effort to implement these methods is very similar (RK23 only requires one more stage than RK12, see Tables 1 and 2) but the computational gain in RK23 is quite substantial. The advantages are not only true in terms of accuracy (as discussed earlier) but also in terms of efficiency (see Figures 8, 9 and 10). For example, to solve the same problem (i.e. Test B with $\Delta\varepsilon_a = 0.01$ and $STOL = 10^{-06}$), the RK12 requires 143 evaluations and only 15 are required for the RK23 (achieving both similar level of accuracy, see Figures 9a and 9b respectively). This trend is even more obvious for more stringent values of *STOL*, with the RK12 needing 1,423 evaluations when $STOL = 10^{-08}$ and RK23 only 68. Similar results are observed for the simpler Test A.

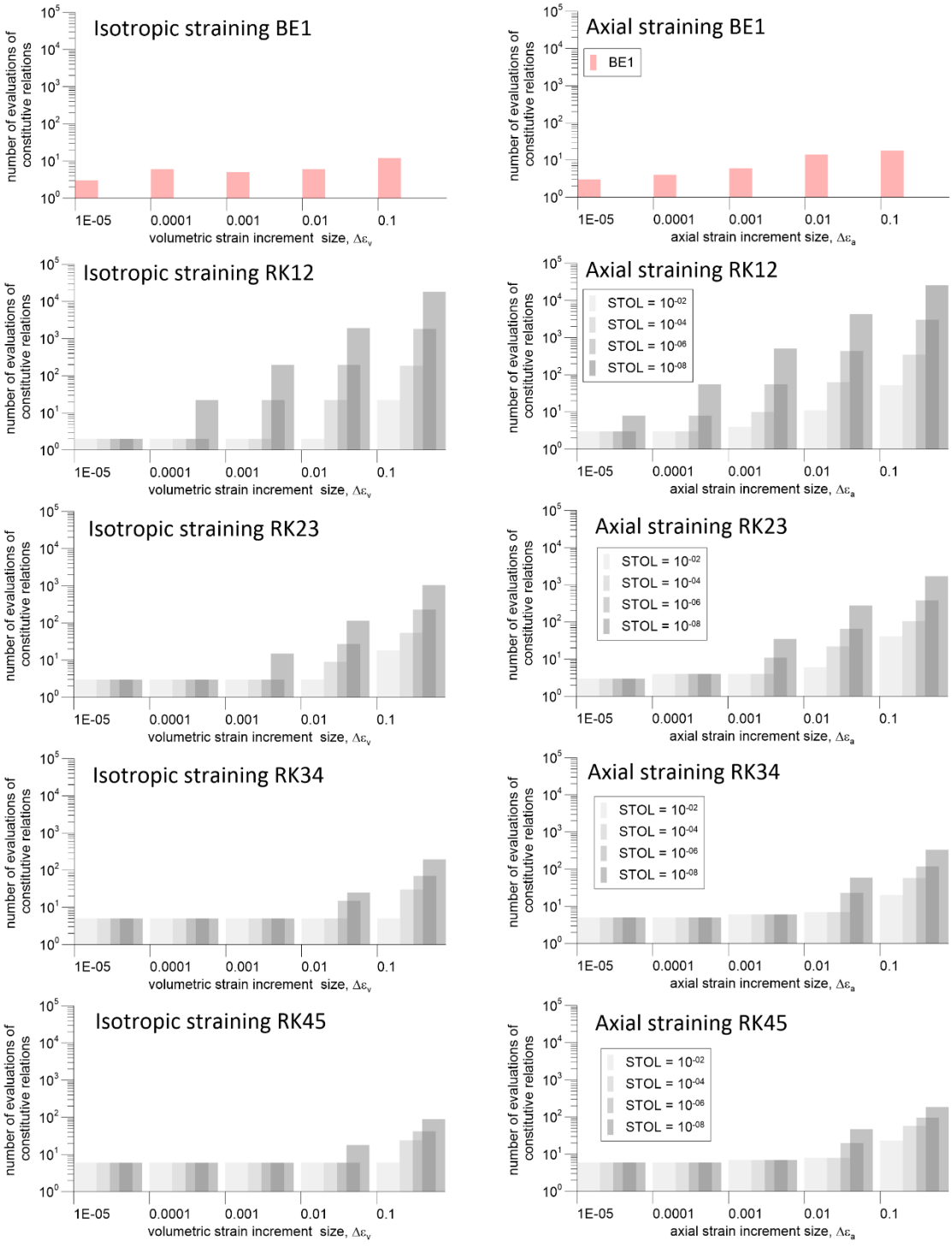

651

652 Figure 10. Computational cost for different *STOL* values against input increment sizes:
653 (left) isotropic straining (Test A); (right) axial straining at constant radial strain (Test
654 B). BE1, 1st order single-step backward Euler; RK12, 2nd order Runge-Kutta with
655 substepping; RK23, 3rd order Runge-Kutta with substepping; RK34, 4th order Runge-
656 Kutta with substepping; RK45, 5th order Runge-Kutta with substepping.

6. CONCLUSIONS

Four explicit substepping integration schemes of different accuracy (including second, third, fourth and fifth order accurate) and one fully implicit first order accurate integration scheme have been implemented to integrate numerically the IVP defined by the initial state and the incremental relations of the Modified Cam Clay (MCC). Their respective numerical performance has been evaluated in terms of accuracy and efficiency to assess which of the five integration schemes is most appropriate to integrate the model.

The implemented integration schemes have been first verified for two numerical tests, including an isotropic straining (Test A) and an axial straining at constant radial strain (Test B). The verification process included the analysis of both: the local relative error incurred in an individual substep and the cumulative relative error incurred over multiple substeps.

As expected, the analysis of the error in solving Tests A and B confirms that poorer accuracies are generally achieved by the first order fully implicit backward Euler (BE1) in line with previous research in the area (Pedroso & Farias, 2005; Potts & Ganendra, 1994). Such differences in accuracy between BE1 and explicit substepping schemes are more noticeable for more stringent values of *STOL* and larger strain increment sizes, at the expense of a higher computational cost (especially for the lower order accurate schemes RK12 and RK23).

The computational performance of the four substepping schemes has been also studied in the context of the performance maps proposed in Lloret-Cabot et al. (2016) to ensure that the accuracy of each substepping scheme is as expected. The analysis of this new form of plotting suggested that the little extra work required in implementing the RK23 (when compared to the implementation of the RK12) is worth the effort because the extra stage that the implementation of the RK23 demands is paid off by the substantial decrease in the number of substeps required to achieve a similar (sometimes even better) accuracy. This suggestion is confirmed when comparing the computational cost of these two substepping schemes. Not only a better accuracy is achieved by the RK23 for a given value of *STOL* and a given increment of strain, but also a considerably lower

number of substeps is typically required, involving reductions in computational cost as large as 90%.

Even though the analysis is based on the numerical results obtained from integrating the MCC most of the conclusions are extrapolatable to the numerical integration of more advanced constitutive models of the critical state family, including critical state models for unsaturated soils, as similar patterns of the local and cumulative relative error are observed (Lloret-Cabot et al. 2021).

7. APPENDIX

For completeness, the behaviour of the error during Test A is included in the Appendix. (see Figure A1, Figure A2 and Figure A3).

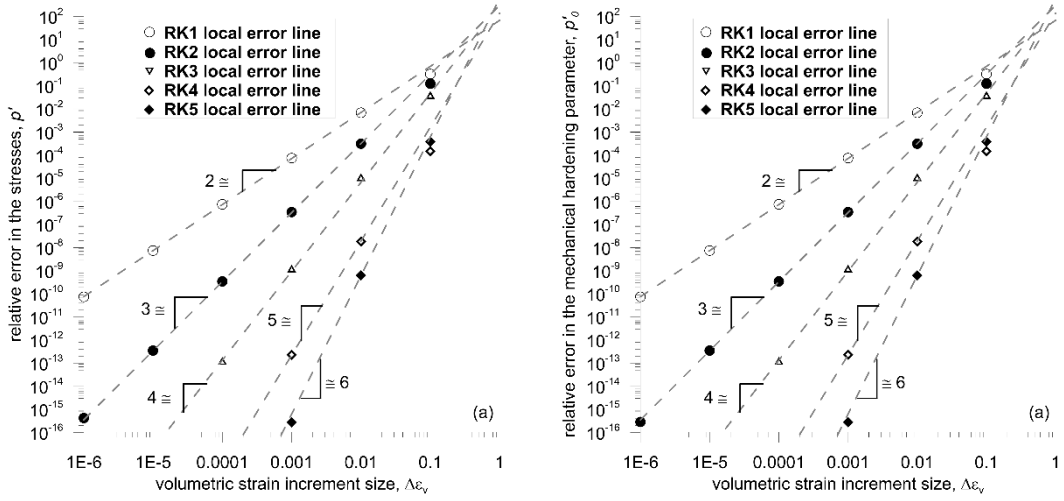

Figure A1. Local relative error against volumetric strain increment size for a single elasto-plastic volumetric strain increment (Test A): (a) effective stress **σ'**; (b) mechanical hardening parameter p_0'. RK1, 1st order single-step Runge-Kutta; RK2, 2nd order single-step Runge-Kutta; RK3, 3rd order single-step Runge-Kutta; RK4, 4th order single-step Runge-Kutta; RK5, 5th order single-step Runge-Kutta.

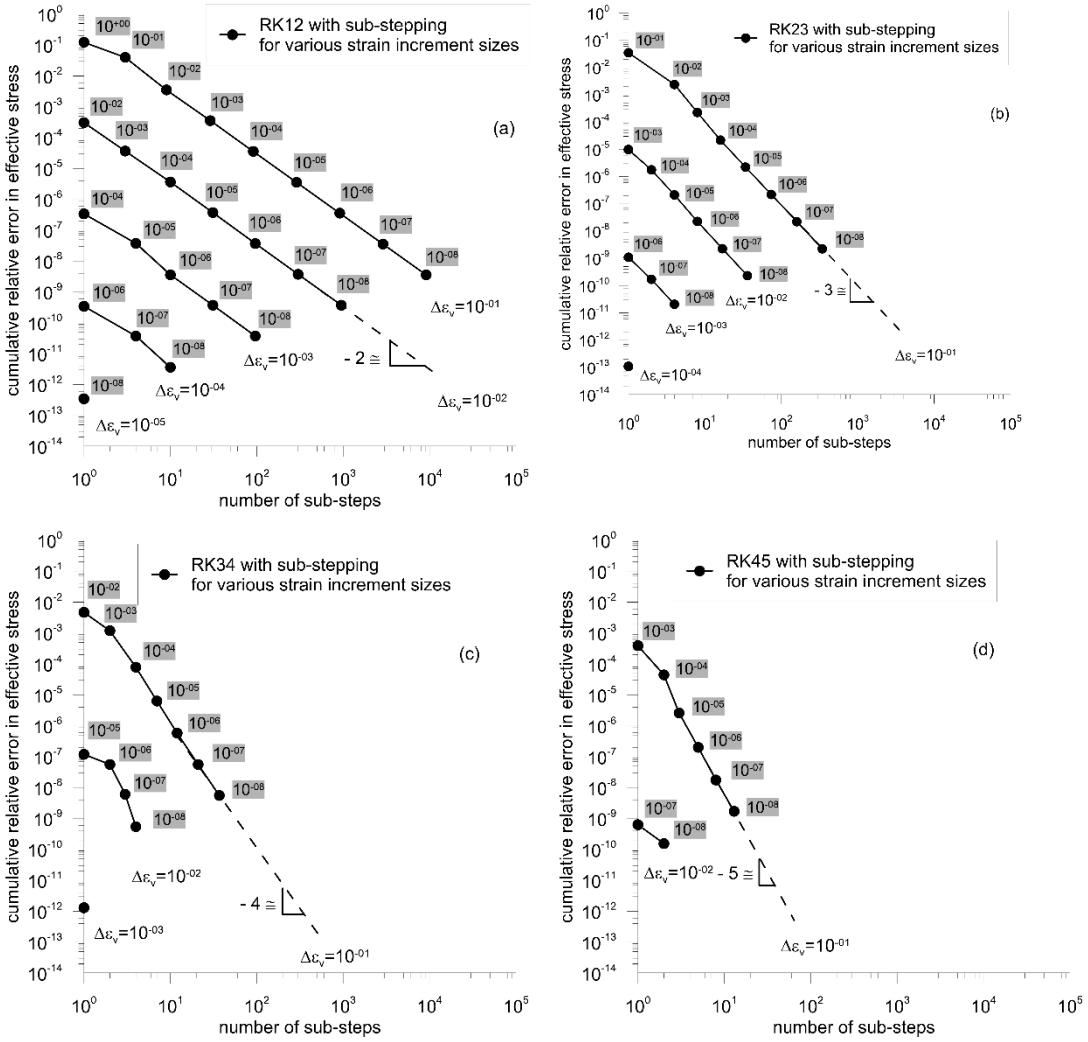

Figure A2. Cumulative relative error behaviour against number of substeps for an elasto-plastic volumetric strain increment (Test A): (a) 2nd order Runge-Kutta with substepping (RK12); (b) 3rd order Runge-Kutta with substepping (RK23); (c) 4th order Runge-Kutta with substepping (RK34); (d) 5th order Runge-Kutta with substepping RK45.

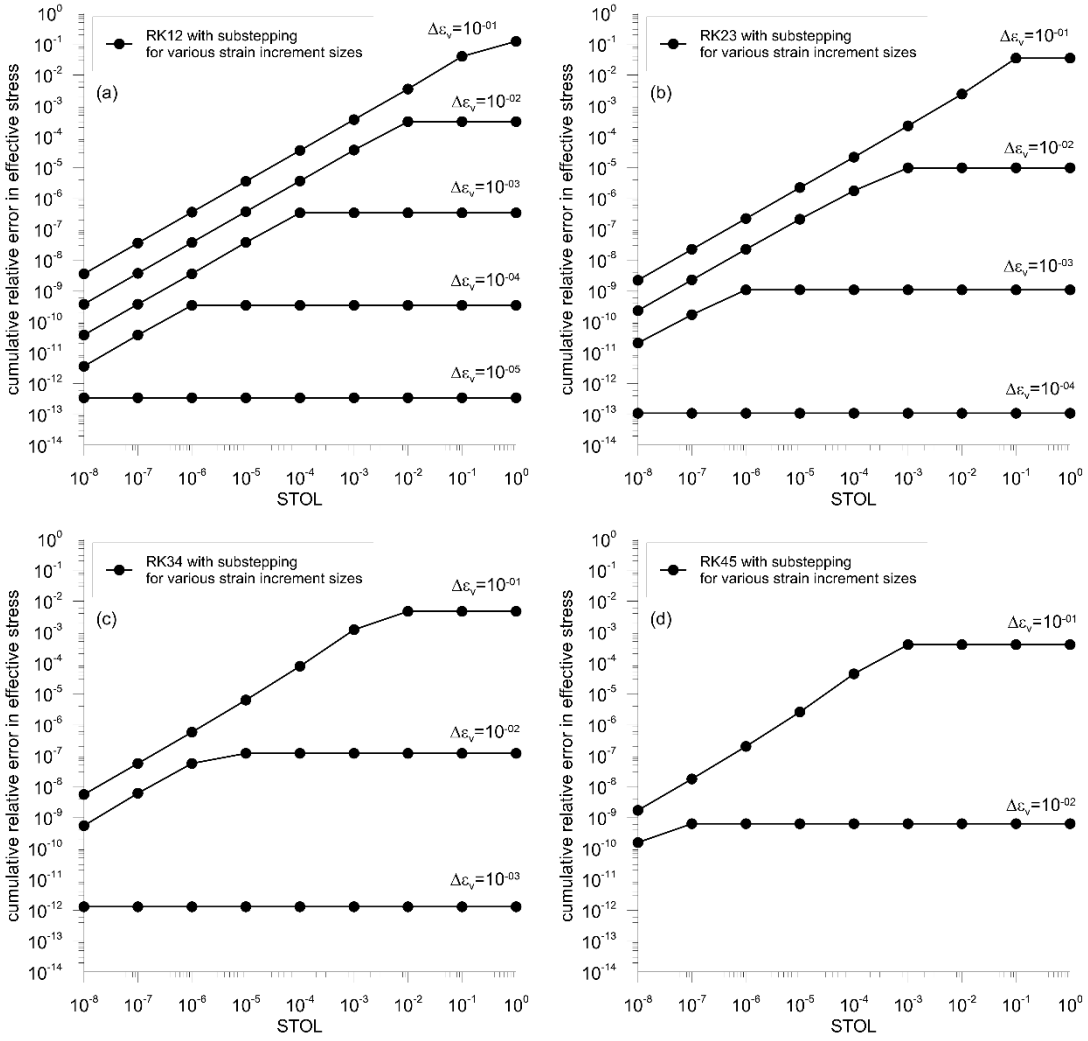

Figure A3. Cumulative relative error behaviour against *STOL* for an elasto-plastic volumetric strain increment (Test A): (a) 2nd order Runge-Kutta with substepping (RK12); (b) 3rd order Runge-Kutta with substepping (RK23); (c) 4th order Runge-Kutta with substepping (RK34); (d) 5th order Runge-Kutta with substepping (RK45).

Note that Figure A2a, A2d, A3a and A3b are equivalent to those presented in Lloret-Cabot et al. (2016).

8. REFERENCES

1. Abbo AJ. An automatic load stepping algorithm with error control. Int. J. Numer. Methods Eng., 39(10) (1996), pp 1737-1759.
2. Alonso EE, Gens A, Josa A. A constitutive model for partially saturated soils. Géotechnique, 40(3) (1990), pp. 405–430.
3. Belytschko T, Liu WK, Moran B. Nonlinear Finite Elements for Continua and Structures. John Wiley and Sons, Chichester, England, (2000).
4. Borja RI, Tamagnini C. Cam-clay plasticity. Part III: Extension of the infinitesimal model to include finite strains. Comput. Methods Appl. Mech. Engrg, 155 (1998), pp. 73-95.
5. Cattaneo F, Vecchia GDella, Jommi C. Evaluation of numerical stress-point algorithms on elastic–plastic models for unsaturated soils with hardening dependent on the degree of saturation. Comp. Geotech., 55 (2014), pp. 404–415.
6. Coombs WM, Crouch RS, Augarde CE. Reuleaux plasticity: Analytical backward Euler stress integration and consistent tangent. Comput. Methods Appl. Mech. Engrg., 199(25–28) (2010), pp. 1733-1743.
7. Coombs WM, Crouch RS. Algorithmic issues for three-invariant hyperplastic critical state models. Comput. Methods Appl. Mech. Engrg., 200(25–28) (2011), pp. 2297-2318.
8. Dormand JR, Prince PJ. A family of embedded Runge-Kutta formulae. Journal of Computational and Applied Mathematics, 6(1) 1980, pp. 19–26.
9. Farias MM, Pedroso DM, Nakai T. Automatic substepping integration of the subloading tij model with stress path dependent hardening. Comput Geotech, 36 (2009), pp. 537-548.
10. Fehlberg E. Low order classical Runge-Kutta Formulas with step-size control and their application to some heat transfer problems. NASA Technical Report 315 (1969).
11. Fehlberg E. Classical fourth- and lower order Runge-Kutta formulas with stepsize control and their application to heat transfer problems. Computing, 6(1-2) (1970), pp. 61-71.
12. Jeremic B, Sture S. Implicit integrations in elasto-plastic geotechnics. International Journal for Mechanics of Choesive-Frictional Materials and Structures, 2 (1997), pp. 165-183.

13. Lloret-Cabot M, Sloan SW, Sheng D, Abbo AJ. Error behaviour in explicit integration algorithms with automatic substepping. Int. J. Numer. Methods Eng., 108(9) (2016), pp. 1030–1053.
14. Lloret-Cabot M, Wheeler SJ, Sánchez M. A unified mechanical and retention model for saturated and unsaturated soil behaviour. Acta Geotech., 12(1) (2017a), pp. 1–21.
15. Lloret-Cabot M, Sloan SW, Sheng D, Abbo AJ. Performance Maps: A Simple Way to Verify the Correctness of Explicit Integration Algorithms with Automatic Substepping. 15th Int. Conf. Intern. Assoc. Comp. Meth. Adv. Geomech. (IACMAG), Wuhan, China, (2017b).
16. Lloret-Cabot M, Wheeler SJ, Pineda JA, Romero E, Sheng D. From saturated to unsaturated conditions and vice versa. Acta Geotech., 13(1) (2018a), pp. 15–37.
17. Lloret-Cabot M, Wheeler SJ, Pineda JA, Romero E, Sheng D. Reply to Discussion of "From saturated to unsaturated conditions and vice versa". Acta Geotech., 13(2) (2018b), pp. 493–495.
18. Lloret-Cabot M, Wheeler SJ, Gens A, Sloan SW. Numerical integration of an elasto-plastic critical state model for soils under unsaturated conditions. Comp. Geotech., (2021), https://doi.org/10.1016/j.compgeo.2021.104299.
19. Pedroso DM, Farias MM. Implicit and explicit numerical integration schemes applied to elastoplastic constitutive laws for soils. In: Proceedings of the 2nd international workshop on new frontiers in computational geotechnics, Gifu University (Japan) and University of Brasilia (Brazil); (2005), pp. 69–81.
20. Pedroso DM, Sheng D, Sloan SW. Stress update algorithm for elastoplastic models with nonconvex yield surfaces. Int. J. Numer. Methods Eng., 76 (2008), pp. 2029–2062.
21. Pérez-Foguet A, Rodríguez-Ferran A, Huerta A. Consistent tangent matrices for density-dependent finite plasticity models, Int. J. Numer. Anal. Meth. Geomech., 25(11) (2001), pp. 1045-1075.
22. Pérez-Foguet A, Rodríguez-Ferran A, Huerta A. Consistent tangent matrices for substepping schemes, Comput. Methods Appl. Mech. Engrg., 190(35-36) (2001), pp. 4627-4647.
23. Potts DM, Gens A. A critical assessment of methods of correcting for drift from the yield surface in elastoplastic finite element analysis. Int. J. Numer. Anal. Meth. Geomech., 9 (1985), pp. 149–59.

783 24. Potts DM, Ganendra D. An evaluation of substepping and implicit stress points
784 algorithms. Comp. Methods in Applied Mech. and Engin. 119 (1994), pp. 341-354.
785 25. Potts DM. Numerical analysis: A virtual dream or practical reality? Géotechnique,
786 53(6), pp. 535-573 (2003).
787 26. Quevedo R, Firme P, Roehl D. Integration schemes with substepping algorithms for
788 creep analysis in geomaterials. Int. J. Numer. Anal. Methods Geomech., 43 (2019),
789 pp. 1467-1487.
790 27. Roscoe KH, Burland JB. On the generalised stress-strain behavior of wet clay. In:
791 Heyman, J., Leckie, F.A. (eds.), Engineering Plasticity. Cambridge University Press,
792 Cambridge, (1968), pp. 535–609.
793 28. Sánchez M, Gens A, Guimarães L, Olivella S. Implementation algorithm of a
794 generalised plasticity model for swelling clays. Comp. Geotech., 35(6) (2008), pp.
795 860–871.
796 29. Shampine LF. Local extrapolation in the solution of ordinary differential equations.
797 Mathematics of Computation, 27(121) (1973), pp. 91-97
798 30. Sheng D, Sloan SW, Yu HS. Aspects of finite element implementation of critical
799 state models. Computational mechanics, 26 (2002), pp. 185–196.
800 31. Sheng D, Sloan SW, Gens A, Smith DW. Finite element formulation and algorithms
801 for unsaturated soils. Part I: Theory. Int. J. Numer. Anal. Meth. Geomech., 27
802 (2003a), pp. 745–765.
803 32. Sheng D, Sloan SW, Gens A, Smith DW. Finite element formulation and algorithms
804 for unsaturated soils. Part II: Verification and Application. Int. J. Numer. Anal.
805 Meth. Geomech., 27 (2003b), pp. 767–790.
806 33. Simo JC, Taylor RL. A return mapping algorithm for plane stress elastoplasticity.
807 Int. J. Numer. Methods Eng., 22(3) (1986), pp. 649–670.
808 34.Sloan SW. Substepping schemes for the numerical integration of elastoplastic stress-
809 strain relations. Int. J. Numer. Methods Eng., 24 (1987), pp. 893–911.
810 35. Sloan SW, Abbo AJ, Sheng D. Refined explicit integration of elastoplastic models
811 with automatic error control. Engineering Computations, 18(1-2) (2001), pp. 121-
812 154. Erratum: Engineering Computations, 19(5-6) (2002), pp. 594–594.
813 36. Sołowski WT, Gallipoli D. Explicit stress integration with error control for the
814 Barcelona Basic Model. Part I: Algorithms formulations. Comp. Geotech., 37(1-2)
815 (2010a), pp. 59–67.

816 37. Sołowski WT, Gallipoli D. Explicit stress integration with error control for the
817 Barcelona Basic Model. Part II: Algorithms efficiency and accuracy. Comp.
818 Geotech., 37(1-2) (2010b), pp. 68–81.
819 38. Sołowski WT, Hofmann M, Hofstetter G, Sheng D, Sloan S. A comparative study
820 of stress integration methods for the Barcelona Basic Model. Comp. Geotech., 44
821 (2012), pp. 22–33
822 39.Zhang Y, Zhou AN. Explicit integration of a porosity-dependent hydro-mechanical
823 model for unsaturated soils. Int. J. Numer. Anal. Meth. Geomech., 40 (2016), pp.
824 2353-2382.
825 40. Zhao J, Sheng D, Rouainia M, Sloan SW. Explicit stress integration of complex soil
826 models. Int. J. Numer. Anal. Meth. Geomech., 29 (2005), pp. 1209–1229.
827 41. Zhao CF, Yin ZY, Hicher PY. Integrating a micromechanical model for multiscale
828 analyses. Int. J. Numer. Methods Eng., 114(2) (2017), pp.105-127.